ADVANCED ELECTRONIC MATERIALS
www.advelectronicmat.de

Flexible Fabrication of Flexible Electronics: A General Laser Ablation Strategy for Robust Large-Area Copper-Based Electronics

Ruzhan Qin, Mingjun Hu, Naibai Zhang, Zhongyue Guo, Ze Yan, Jiebo Li, Jinzhang Liu, Guangcun Shan,* and Jun Yang*

Attributed to high power density and controllable digital program operation, lasers are a powerful tool in the preparation, prototype fabrication, and post-processing of materials. In this paper, a general laser ablation strategy that can be conducted under ambient, room-temperature, and mask-free conditions is employed for the rapid fabrication of robust large-area copper-based flexible electronics. Micrometer-scale thick copper layer cladded on flexible polymer substrate can be removed efficiently in one laser scanning pass based on laser-induced heat evaporation effect. Metal grids with a width less than 10 microns and a thickness close to 2 microns can be produced in a reliable manner. As proof-of-concept demonstrations, flexible transparent conducting electrodes and a variety of flexible circuit boards (FCBs) with different precisions and dimensions are fabricated by this approach in a digitally controlled mode and their photoelectric properties under normal and deformation states are investigated. The results indicate that the method is robust and as-prepared flexible electrodes and circuits are reliable and endurable, indicative of the potential of this method in scalable fabrication of sub-millimeter flexible electronics through a straightforward and flexible fashion.

1. Introduction

In recent years, flexible wearable and portable electronic products that can meet various special needs have gained rapid growth and received widespread attention.[1] Flexible electronic devices, including flexible sensors,[2–4] flexible transistors,[5] flexible supercapacitors,[6,7] flexible nanogenerators,[8] flexible screen panel,[9] flexible light-emitting diodes,[10] flexible photodetectors,[11] flexible thin-film solar cell,[12] etc., are developing toward flexibility, intelligence, and high integration, and the materials with good photoelectric performance, excellent processibility, low cost, good reliability, and chemical stability are highly desirable.

Compared with traditional rigid devices, flexible electronics can adapt to different working environments and meet the requirements of various deformations while maintaining the normal functions of electronic devices. In flexible photoelectric devices, the flexible transparent conducting electrodes (FTCEs) are an indispensable part, and currently the most widely used FTCE is indium tin oxide (ITO)-coated transparent plastic film. However, ITO coated film has the following shortcomings: high cost of indium, large material waste in the production process, the requirement of expensive high-vacuum equipment, and the most important one—intrinsic brittleness of ITO, which is incompatible with the future low-cost wearable flexible electronic devices.[13] In order to develop inexpensive and reliable alternatives of ITO, many novel materials and fabrication methods have been put forward. Metal nanowires (NWs) are considered to be the most promising alternatives of ITO for fabricating high-performance FTCEs.[13] Recently, silver nanowires mesh structures have been widely employed as conductive layer on flexible transparent substrate, and superior light transmission and conductivity have been obtained. More importantly the performance degradation of

Dr. M. Hu, Dr. J. Liu
School of Materials Science and Engineering
Beihang University
Beijing 100191, China
E-mail: mingjunhu@buaa.edu.cn

R. Qin, Z. Yan, Prof. G. Shan
School of Instrumentation Science and Opto-electronics Engineering
Beihang University
Beijing 100191, China
E-mail: gcshan@buaa.edu.cn

The ORCID identification number(s) for the author(s) of this article can be found under https://doi.org/10.1002/aelm.201900365.

DOI: 10.1002/aelm.201900365

Dr. N. Zhang
Beijing Research and Development Center
the 54th Research Institute
Electronics Technology Group Corporation
Beijing 100070, China

Z. Guo, Dr. J. Li
Beijing Advanced Innovation Center for Biomedical Engineering
School of Biological Science and Medical Engineering
Beihang University
Beijing 100191, China

Prof. J. Yang
Beijing Institute of Nanoenergy & Nanosystems
Chinese Academy of Sciences
Beijing 100083, China

the film under repeated deformation is much less than ITO-based flexible films. However, silver has relatively high material cost. Compared with silver, copper is 90 times cheaper and has nearly as good conductivity as silver.[9] The best performance of the current reported copper nanowires-based films is the transparency of 96% and the sheet resistance of 0.1 Ω sq^{-1},[14] and thus copper is a good substitution for silver to further reduce materials cost. In addition to metal nanowires, electrospun metal nanofiber is also a fantastic material to build conductive mesh layer on flexible substrate attributed to extremely large aspect ratio of electrospun nanofiber.[15–17] However, nanowire-based and nanofiber-based metal electrodes require complex material synthesis and delicate post-treatment annealing steps due to high resistance between nanowire/nanofiber junctions. Attributed to mismatched post-processing temperature of metal and polymer, how to selectively weld the inter-wire junctions and remove isolated organic components while not causing the unrecoverable plastic deformation of polymer substrate under high temperature has been an important issue to improve the conductivity of FTCEs.[9,18,19] In contrast to metal nanowires, regular metal grid mesh is another kind of promising transparent electrode material. This kind of structure has several advantages: controllable microstructure design, low junction resistance, and uniform and reliable optical/electrical properties. So far, a lot of methods have been proposed for the fabrication of regular metal grid mesh films, typically including laser sintering,[20–23] various lithography techniques,[24–29] nanoimprinting,[30] laser direct synthesis,[31] contact printing,[32] jet printing,[33,34] laser printing,[35] evaporative assembly,[36] breath-figure template,[37] etc. Recently, Paeng et al. adopted nanosecond laser to selectively ablate 19 nm thick copper layer coated on PEN film and obtained copper-based FTCEs with regular hole arrays. As-prepared films showed light transmission of 83% and sheet resistance of 17.48 Ω sq^{-1}.[38] They ascribed the formation of ablated holes to outward radial flow of dewetted molten copper and the ejection of molten copper under high power laser irradiation, and it seems that such laser ablation technique is just suitable for the preparation of metal mesh-type FTCEs with ultrathin metal layer and high areal filling ratio due to poor flowability of molten metal. Herein, we proposed a kind of laser-induced metal evaporation method to selectively remove metal layer on flexible substrate for one-step fabrication of metal pattern. This method is more suitable for the removal of thick metal layer than that described by Paeng et al. because the evaporation is a more effective physical removal process than melt ejection and dewetting. Thus, this method is not only compatible with the fabrication of highly conductive FTCEs, and can also be used for the preparation of the FCBs with large metal layer thickness that possessed high power supplying ability for running a variety of high-power electronic components.

In this study, a 3W UV laser with the excitation wavelength of 355 nm was used to ablate copper on flexible polymer in consideration of strong light absorption of copper in UV waveband. Attributed to high laser energy density and light-heat conversion efficiency, UV laser can quickly vaporize surface copper layer without causing obvious thermal damage to the underlying flexible polymer substrate. In this method, micrometer-scale thick copper layer can be directly removed under ambient conditions while leaving clean and smooth polymer surface. Flexible copper patterns with different precisions and dimensions were obtained in a highly flexible and digitally controlled mode. The study indicated that our proposed UV laser ablation method based on metal evaporation is a general strategy for fabricating robust large-area metal-based flexible electronics. As a proof-of-concept demonstration, this method was adopted for preparing copper-based FTCEs. As-prepared Cu grid-type FTCEs could show optimal optoelectrical performance (sheet resistance: 21.6 Ω sq^{-1}, light transmission at 550 nm: 90.9%), and behaved as the display of electroluminescent light emitter. Also, such films can be applied as transparent electromagnetic interference (EMI) shielding materials in some special fields where high light transmission and EMI shielding ability were both required. In addition, this method could also be employed to produce various FCBs with excellent electrical properties and mechanical flexibility. It should be the first straightforward description of laser ablation method for the fabrication of micrometer-scale thick copper-based patterns on flexible transparent polymer substrates.

2. Result and Discussion

Figure 1 showed the schematic of laser ablation method for the fabrication of typical Cu grid FTCEs. A desired functional pattern was designed by drawing software and then imported into laser processing software. Then, the laser cutting operation was executed following the given laser parameters under computer assistance. The unwanted copper layer was removed by high power laser and the left copper patterns form the required metal network to achieve the specified function. Herein, UV laser was selected to ablate copper because copper can exhibit a stronger absorption in UV region than that in other light wavebands,[39] and thus can enhance laser ablation efficiency. In our method, the power of the UV laser used to ablate copper was 3 W, of which about 1.5 W could be received by copper surface, and about 75% of as-received laser power was absorbed by copper layer, and when the laser spot diameter was close to 8 μm, the surface laser power density was in the order of 10^6 W cm^{-2}. Based on the spatiotemporal heat-conduction equation,

$$\frac{1}{k}\frac{\partial T}{\partial t}=\frac{\partial^2 T}{\partial x^2}+\frac{\partial^2 T}{\partial y^2}+\frac{\partial^2 T}{\partial z^2} \tag{1}$$

we can get to know the temperature distribution in copper layer during laser illumination. In this equation, k is the thermal diffusivity, T represents the temperature, t is the time, and x, y, z are orthogonal coordinates. And $k=\frac{K}{\rho c}$, in which K is the thermal conductivity of copper, ρ is the mass density, and c is the specific heat capacity of copper. In this case, we approximately considered laser heating of copper layer as homogeneous heating mode of semi-infinite solid metal, and the heat transfer through copper layer was deemed as 1D heat conduction mode, and thus the temperature gradient in copper layer can be expressed as follows:

$$P_s=-K\frac{\partial T}{\partial z} \tag{2}$$

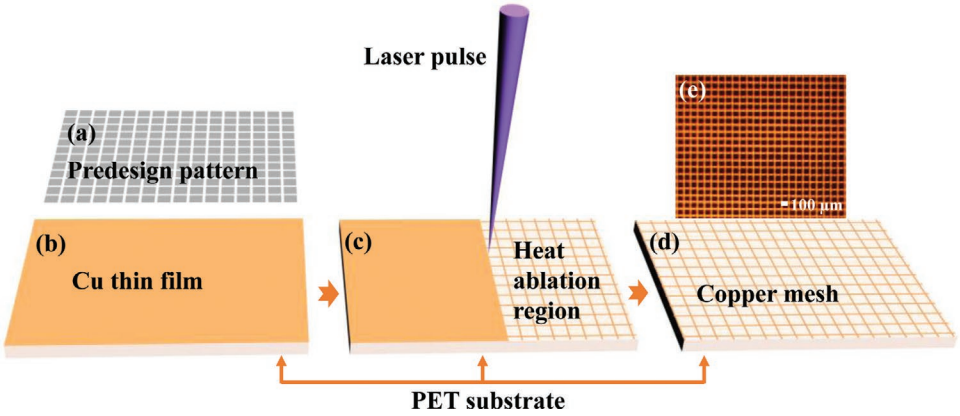

Figure 1. Schematic illustrations of fabrication process of Cu FTCEs. a) Predesign pattern made by drawing software. b) The prepared copper clad flexible polyethylene terephthalate (PET) film. c) Laser ablation process for fabricating various metal patterns. d) As-prepared copper patterns after laser ablation. e) Optical microscope image of real copper pattern prepared by laser ablation method.

the solution of the heat conduction equation can be given as

$$T(z,t) = \frac{2P_s}{K}\sqrt{kt}\ \ ierfc\left(\frac{z}{2\sqrt{kt}}\right) \tag{3}$$

where, $\text{ierfc}(x) = \int_x^\infty erfc(u)\,du$, $\text{erfc(u)} = \frac{2}{\sqrt{\pi}}\int_u^\infty \exp(-s^2)\,ds$, $P_s = P_{s0}(1-\rho_R)$, in which ρ_R is the reflectivity of laser, and P_{s0} is the power density of incident laser. When $z = 0$,

$$T(0,t) = T_s - T_0 = \frac{2P_s\sqrt{t}}{\sqrt{\pi K\rho c}} \tag{4}$$

in which, T_s represents the surface temperature of copper layer after time t, and T_0 denotes the initial temperature of copper surface layer. Thus, it is easy to get a rough time to achieve the boiling point of copper under UV laser illumination. It is calculated that to convert surface copper from the initial solid to melt to gas only needs about one third of a pulse width (≈30 μs), and thus there is enough time to allow copper to evaporate during a pulse width. Therefore, in our laser ablation case, copper vaporization is the dominant copper escaping style. In addition, the vaporization rate of copper can also be estimated by the following equation,

$$\frac{dz(t)}{dt} = v = \frac{P_s}{\rho[L + c(T_b - T_0)]} \tag{5}$$

where v is the vaporization rate, L is the latent heat of phase change, including melting and vaporization, and T_b is the boiling point of copper. In this case, the typical copper vaporization rate v can achieve several hundred nanometers per microsecond. The typical used laser pulse width is 30 μs, and thus several micrometers cutting depth can be easily achieved in this case.

Figure 2 showed optical microscope images and SEM images of Cu FTCEs with different microstructures and sizes. Figure 2a,b displayed two round hole arrays with different hole diameters, and in these two cases the size of the ablated holes was determined completely by the laser power. When the power was ≈0.8 W, the small round holes arrays with the hole diameter of about 5 μm could be well formed on flexible substrates, and when the power was increased to 1.1 W, the dimension of the ablated hole was extended largely and the hole diameter was enlarged to 30 μm. More precise size control could be accomplished by the combined action of laser power and software program. Figure 2c–f is the optical microscope images of copper grid mesh electrodes (200 nm thick) with different grid sizes (all copper line widths were set at 40 μm, and the grid spacings were set at 50, 100, 200, and 400 μm, respectively). The corresponding SEM images of Cu FTCEs are shown in Figure 2g–j. It can be seen basically the unwanted copper layer on PET film has been fully removed after one-pass laser scanning, and the edge of the left copper layer is clean and approximately smooth, with slight zigzag wave. In the laser ablation area, shreds of impurities and a small amount of residual copper particles can also be seen, and they are distributed sparsely on the flexible substrate with little influence to light transmission and conductivity. The zoom-in SEM images to reflect laser ablated boundaries of 200 nm thick copper layer on PET were presented in Figure S1a–c, Supporting Information. After laser ablation, the remained metal line width was far less than the set value of 40 μm, even less than 20 μm, which was associated with laser spot size (≈8 μm) and heat affected zone. With further decreasing the set value of line width, the obtained real size of copper line width can be further decreased. In Figure 2k, parallel copper line arrays with a line width only about 6 μm can be acquired by selecting appropriate laser parameters and the initial set value of line width, and even some smaller line widths can be achieved with the further optimization of processing parameters (Figure S2, Supporting Information).

As shown in Figure 2g–j, the average widths of the ablated copper lines are about 16.7, 16.7, 22.3, and 23.9 μm, respectively, and the corresponding space areas are 73.3 μm × 73.3 μm, 123.3 μm × 123.3 μm, 217.7 μm × 217.7 μm, and 417.1 μm × 417.1 μm, respectively. Therefore, the area filling ratio of the left copper pattern on the polymer film are 33.7%, 22.4%, 17.7%, and 10.1% for the four different copper grid mesh films. The less area filling ratio of copper pattern will result in higher transparency of the film. Figure 2l present the digital photos of

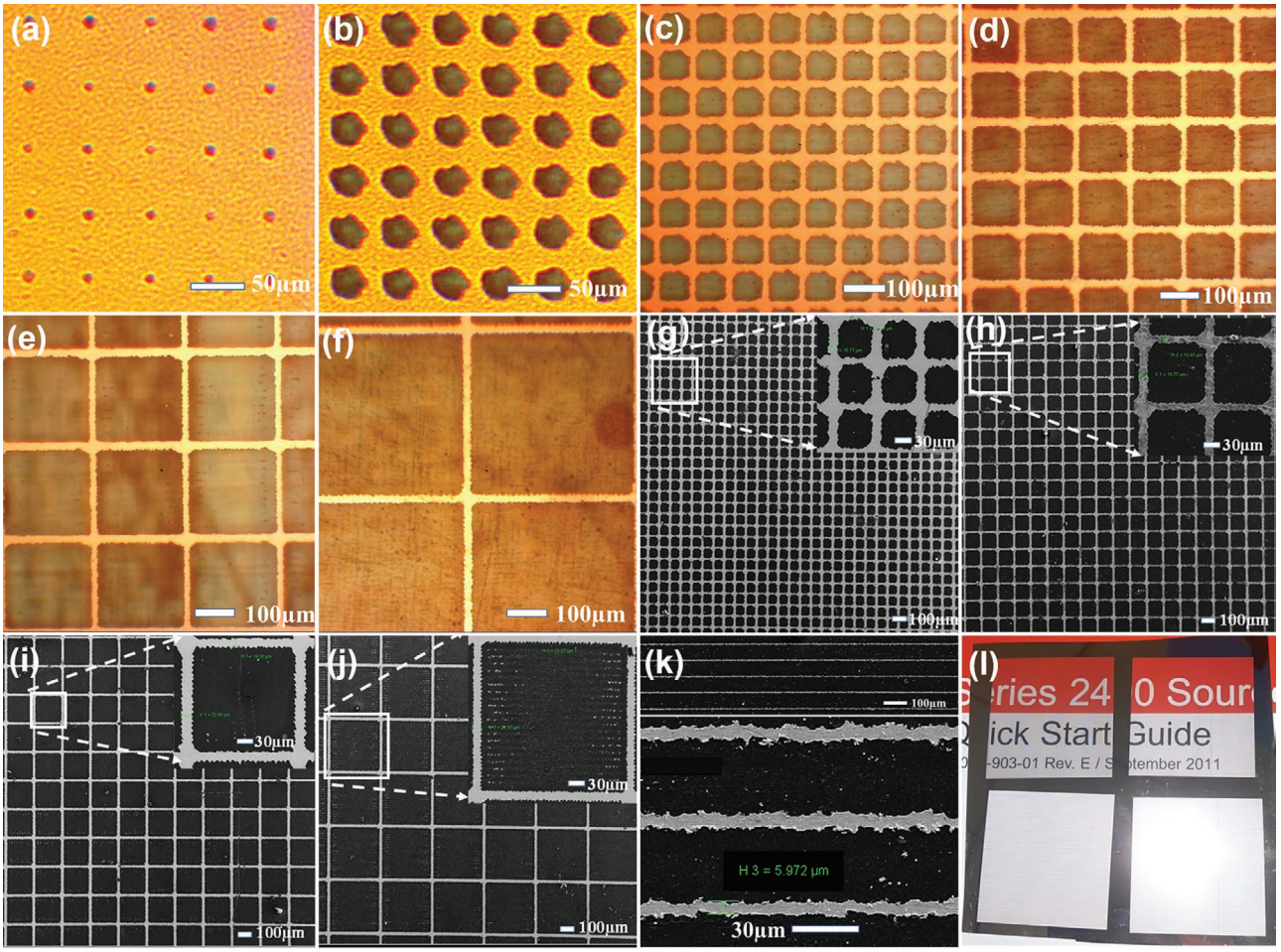

Figure 2. a,b) Optical microscope image of different copper hole arrays (a: small hole arrays; b: large hole arrays) after laser ablation with different power (a: 0.8 W; b: 1.1 W); c–f) Optical microscope image of Cu FTCEs with different predesign grid spacings (c, 50 μm × 50 μm; d, 100 μm × 100 μm; e, 200 μm × 200 μm, f, 400 μm × 400 μm). g–j) SEM images of Cu FTCEs after laser ablation with different predesign copper grid spacings (g, 50 μm × 50 μm; h, 100 μm × 100 μm; i, 200 μm × 200 μm; j, 400 μm × 400 μm) and the locally zoom-in SEM images in the upper right inset. k) SEM images of parallel copper lines; l) The digital photos of Cu FTCEs with different microstructures to show the transparency of as prepared transparent conductive film in such laser ablation methods (left top, right top, left down, and right down transparent windows corresponding to different predesigned copper patterns with the same copper line width (40 μm) and different pitches (50, 100, 200, and 400 μm). In all images, the thickness of copper layer is 200 nm.

several typical copper-based grid mesh films, and good transparency can be observed. In this film, four transparent windows correspond to four kinds of different copper grid patterns with different nominal grid space sizes: 50 μm × 50 μm (upper left), 100 μm × 100 μm (upper right), 200 μm × 200 μm (left lower), 400 μm × 400 μm (right lower), respectively. The transparency was investigated by UV–vis-NIR spectra, which is shown in **Figure 3**a. The light transmissions at 550 nm are 64%, 72.6%, 81.6%, and 90.9%, respectively, and the corresponding sheet resistances are 4.5, 6.6, 10, and 21.6 Ω sq^{-1}, respectively. The combined properties are comparable with and even superior to most of copper nanowires-based electrodes and ITO conductive glass (Figure 3b).

Like other reports, we also employed Figure of Merit (FoM) to evaluate the comprehensive optoelectrical performance of as-prepared copper grid FTCEs.[45,46] Figure of Merit (FoM) of transparent conductive film can be expressed by the following equation, and denotes the ratio of DC electrical conductivity σ_{dc} over optical conductivity σ_{opt}.

$$\mathrm{FoM} = \frac{\sigma_{dc}}{\sigma_{opt}} = \frac{188.5}{R_s\left(\frac{1}{\sqrt{T}} - 1\right)} \tag{6}$$

where R_s and T are the sheet resistance and light transmittance of the copper grid electrodes. When T is considered as the light transmission at 550 nm, FoMs of 200 nm thick Cu FTCEs were calculated to be ≈168, 165, 201, and 179, respectively, which are better than many other reported transparent electrodes, such as ITO,[47] graphenes,[48] CNTs,[49] copper nanowires,[50] metal grid meshes,[51,52] etc. To continuously increase the FoMs, the thickness of copper layer needs to be further increased. We also investigate the light transmission and conductivity of 2 μm thick copper grid mesh films. Copper FTCFs was ablated

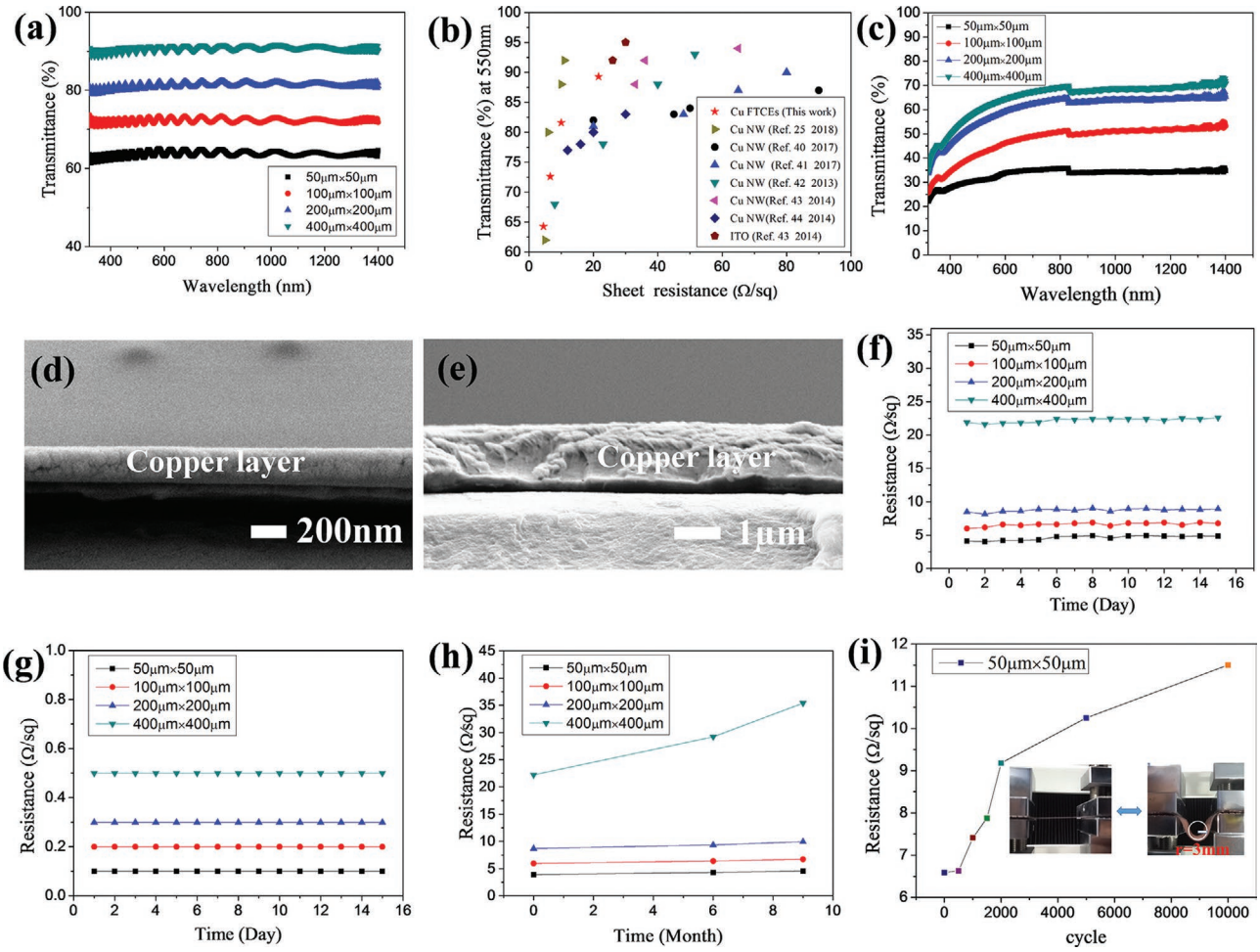

Figure 3. a) The UV–vis-NIR spectra of 200 nm thick Cu FTCFs with different copper grid spacings after laser ablation. b) Optoelectronic performance comparison of Cu FTCEs (200 nm thick) prepared by our method with other Cu NWs-based transparent conductors and ITO.[25,40–44] c) The UV–vis-NIR spectra of 2 μm thick Cu FTCEs with different copper grids spacings. d) SEM image of cross section of 200 nm thick copper film. e) SEM image of cross section of 2 μm thick copper film. f) The oxidation stability of 200 nm thick Cu grid FTCEs under ambient conditions within 15 day. g) The oxidation stability of 2 μm thick Cu grid FTCEs under ambient conditions within 15 day. h) The long-term oxidation stability of 200 nm thick Cu grid FTCEs under ambient conditions within 9 months. i) Sheet resistance variation of 200 nm thick copper grid FTCEs in 10000 times cyclic bending test.

by UV laser based on the same method merely with the promoted ablation power. In contrast to 200 nm thick copper layer, the removal of 2 μm thick copper layer is much more difficult might due to the significantly enhanced heat accumulation in thick copper layer resulting in the softening of polymer substrate which render the adhesion between copper and polymer increased. After laser ablation, for 2 μm thick copper film, the polymer surface layer in the laser ablated area is not very clean and transparent any more like that in 200 nm thick copper layer case, but became a little dirty and obscure, presenting the signs of partly melting and even carbonizing, indicating that the polymer surface layer has started to be broken by the heat effect of UV laser (Figure S1d–f, Supporting Information). Although with the limited film quality, a series of flexible transparent conductive films with specific optoelectrical performance could be still obtained. The optical microscope images and SEM images of as-prepared 2 μm thick copper grid mesh films with the nominal line width of 40 μm and different nominal grid space areas (50 μm × 50 μm, 100 μm × 100 μm, 200 μm × 200 μm and 400 μm × 400 μm, respectively) are presented in Figure S3a–h, Supporting Information. Figure 3c showed the optical transmittance of these films are 31.5%, 43.6%, 56.7%, and 62.3%, respectively, far less than the 200 nm thick copper film. However, the film conductivity was improved markedly, with the sheet resistance of 0.1, 0.2, 0.3, and 0.5 Ω sq^{-1}, and thus FoMs of 2 μm thick copper FTCFs dramatically increased and became 2411, 1832, 1915, and 1412, respectively. Such high FoMs are mainly attributed to low sheet resistance, and if the light transmission was enhanced, the FoMs should be further improved. Currently poor optical transmittance of 2 μm thick copper grid film was principally derived from the unremoved metal residuals and unsmooth polymer surface. Therefore, in next plan, cleaning up the surface copper layer fully while keeping the polymer substrate intact is a necessary way for further raising optoelectrical performance of the film.

In our experiments, the copper clad PET films were prepared by vapor deposition or sputtering deposition (Figure 3d,e), and thus the obtained copper layer has a good adhesion to polymer

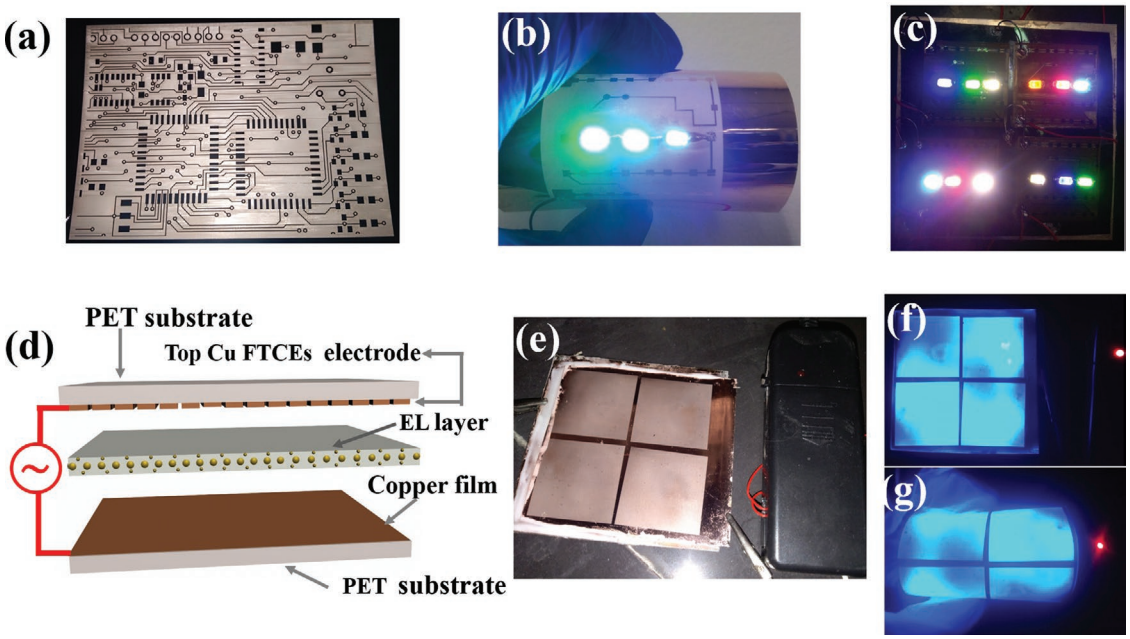

Figure 4. a) The digital photo of a typical flexible circuit board fabricated by laser ablation method; b,c) The LED installed flexible circuits work well under normal and bending deformation; d) Schematic of the sandwiched structure of the EL light emitter; e) optical photograph of as-prepared flexible EL light emitter using Cu grid FTCEs as electrode; f) normally running EL light emitter; g) the running EL light emitter under bending deformation.

substrate as well as presents a good crystallinity (Figure S3i, Supporting Information). Highly crystalline copper possesses fewer lattice defects and grain boundaries, and thus can show better oxidation resistance than copper nanoparticles or electroless plating copper. Figure 3f–h show the oxidation stability of the Cu FTCEs with different copper thicknesses and grids space areas under ambient conditions. As can be seen from the Figure 3f–g, the resistance changes little within half a month. With further increasing the standing time of copper grid films to nine months under atmosphere, the resistance of the copper mesh films with a larger grid spacings increased slightly, which might be related to slight edge oxidation. For the film with higher surface copper coverage, the effects of the oxidized edges on the total conductivity is negligible and thus the curves basically keep unchanged even after nine months, showing a superior oxidation resistance. The electrical properties of copper grid films under mechanical deformation were also investigated. The 200 nm thick Cu mesh transparent conductive films with the nominal grid space area of 50 μm × 50 μm were used for this test, and the test results were shown in Figure 3i. The initial sheet resistance of the film is measured to be 6.59 Ω sq^{-1}, and then becomes 6.63 Ω sq^{-1} after 500 bending cycles at bending radius of 3 mm. In the bending tests, tensile and compressive stresses could be induced in a controlled mode. The bending strain could be calculated by the equation $\varepsilon = t_s/(2r)$, where t_s is the substrate thickness (125 μm) and r is the bending radius, and thus ε = 2.1%. In the whole bending process, the relative resistance variation ($\Delta R/R_0$) was maintained within 1% in each cycle, and electrical and mechanical failure was not observed even after 10 000 bending cycles, which signifies that the films have good combination properties of mechanical strength and electrical conduction as well as excellent resistance to bending fatigue. In addition, copper clad PET films also show good electrical performance maintenance under large strain during repeated bending cycles, and even after a handful of 180° bending cycles, no failure happens (Figure S4, Supporting Information). These properties are much better than ITO based flexible conductive films, and such excellent mechanical and electrical properties primarily ascribed to strong adhesion of copper layer to flexible substrate and good crystallinity that resulted in good conductivity under various deformations.

In addition to preparing flexible transparent electrodes with different optoelectrical performance, the laser ablation methods were also very suitable for the fabrication of various FCBs on account of flexible digital design and operation (Figure S5, Supporting Information). As shown in **Figure 4**a, a typical FCB was obtained based on our laser ablation method. The ablation process can be finished within several minutes. Different from conventional chemical etching method, photoresist and mask is not necessary in such method, and the FCB can be produced in one laser scanning pass, avoiding the sophisticated multistep operation in conventional circuits fabrication. Figure 4b,c shows that as-prepared FCBs can well function as electrical connector to supply power sources for lighting a series of LED and guarantee their normal running even under large bending, twisting and folding deformations.

As proof-of-concept demonstration, the prepared copper grid transparent conductive films were adopted to act as the electrode of electroluminescent (EL) light emitters. The EL emitter had a typical sandwiched structure configuration, with active middle layer and two flexible electrodes (Figure 4d). The active middle layer was mainly composed of ZnS: Cu/Al nanoparticles, and small amount of PDMS was used as adhesives to make active

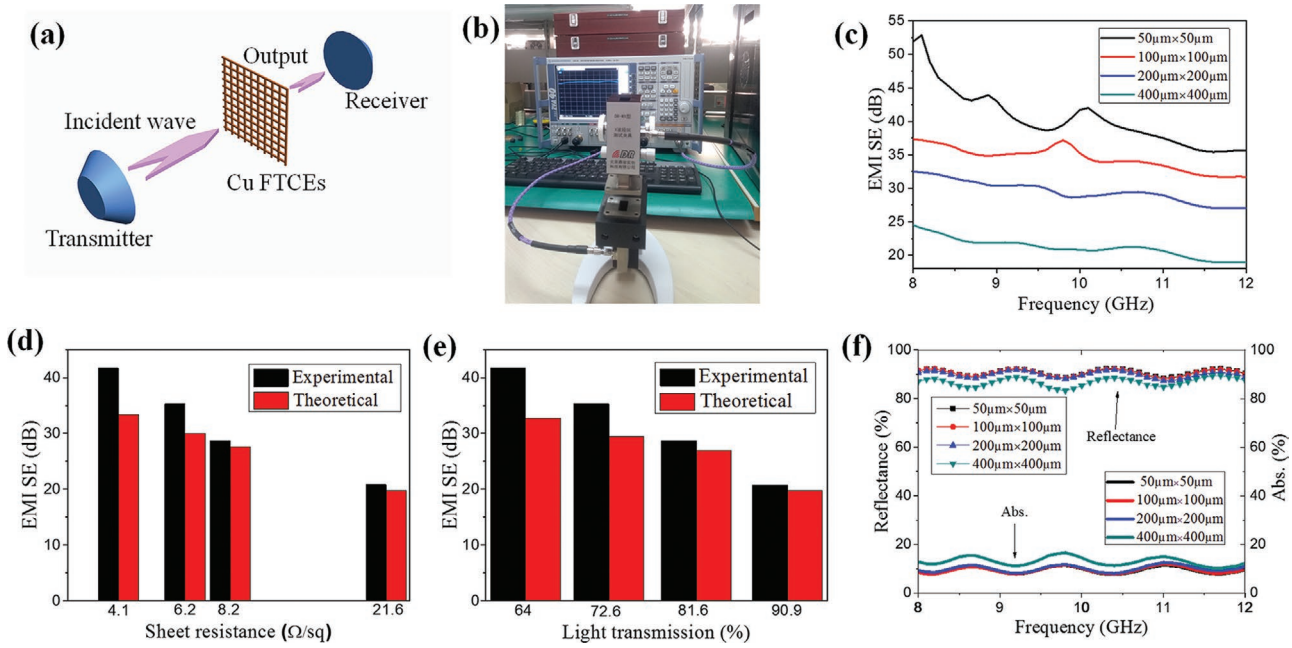

Figure 5. a) Schematic illustration of the EMI SE measurement setup. b) The waveguide setup for EMI SE measurement. c) EMI SE curves of the 200 nm thick Cu grid FTCEs with different copper areal filling ratio in the frequency band of 8–12 GHz. d) The experimental and calculated EMI SE values of copper grid FTCEs versus sheet resistance. e) The experimental and calculated EMI SE values of copper grid FTCEs versus light transmission. f) Reflection and absorption percentage of electromagnetic wave through copper grid FTCEs with different grid spacings in X-band.

EL layer keep good conformal contact with the two flexible electrodes. In the EL emitter, top flexible electrode layer is the copper grid FTCEs prepared by our laser ablation method, and the bottom electrode layer is copper clad PET. A typical assembled EL emitter was shown in Figure 4e. The active EL nanoparticles were excited by an AC voltage and emitted bright blue light (Figure 4f), and even under large bending deformation, the emitter can work very well (Figure 4g), indicating that our metal grid transparent electrodes can offer low sheet resistance and be used in flexible EL displays.

In consideration of the superior optical transparency and electrical behavior, the Cu FTCEs may also be used as transparent EMI shielding material, which is becoming more and more important in some special applications, such as transparent windows of spacecraft, radiation-proof flexible displays, touch panels, wearable electromagnetic devices, etc.[53] attributed to the integration of high transparency and EMI shieling ability. In our experiments, EMI SE measurement of copper FTCFs was executed on a typical waveguide setup, which is mainly composed of three components: transmitter antenna, X-band waveguide and receiver antenna as shown in **Figure 5**a,b. The electromagnetic interference shielding effectiveness (EMI SE) of as-prepared films was calculated by the following expressions,[54–56]

$$\text{Total EMI SE} = 10\log\left(\frac{P_i}{P_t}\right) = 10\log\left(\frac{1}{|S_{21}|^2}\right) \quad (7)$$

where P_i is the power of incident electromagnetic wave, P_t is the power of transmitted electromagnetic wave, and $|S_{ij}|^2$ is the ratio of the transmitted powers of port i to port j. Figure 5c showed EMI SE values of as-prepared copper grids films with different copper areal filling ratios, and at 10 GHz EMI SE can reach 41.7, 35.3, 28.7, and 20.8 dB, respectively, with decreasing copper grid coverage. It can be seen that even for the films with the sheet resistance of 21.6 Ω sq^{-1} and light transmission of 90.9%, EMI SE is still kept above 20 dB, which has achieved the basic requirement for household appliances. However, to meet the military requirements, at least 80 dB EMI SE value should be achieved while keeping optical transmittance above 80%, and thus there is still a long way to walk for the development of flexible transparent EMI shielding film with ultrahigh SE and great transparency for military purpose. By further increasing the thickness of metal grids, the EMI SE value can be improved, and over 50 dB EMI SE at 10 GHz is obtained when the copper layer thickness is 2 μm as a result of the improved conductivity derived from increased copper thickness (Figure S6a–c, Supporting Information), however with great loss of light transmission for our laser ablation method due to unclean polymer surface with residual copper.

In our conductive film case, because the thickness of conductive layer is far less than skin depth of electromagnetic wave ($d \ll \delta$), the following formula can be given,[55,57,58]

$$\text{EMI SE} = 20\log\left(1+\frac{Z_0}{2R_s}\right) \quad (8)$$

in which, Z_0 is the impedance of free space (377 Ω) and R_s is the sheet resistance of the conductive film. Figure 5d showed contrast diagram of the experimental EMI SE and the theoretical EMI SE values calculated by Equation (8), and it was found the results matched well in higher sheet resistance range (>8.2 Ω sq^{-1}).

In combination with Equation (6), the EMI SE can also be written as the function of the transparency T as follows:

$$\text{EMI SE} = 20\log\left[1+\frac{\sigma_{dc}}{\sigma_{opt}}(T^{-0.5}-1)\right] \quad (9)$$

in which, T is the light transmission at 550 nm, and $\frac{\sigma_{dc}}{\sigma_{opt}}$ is FoM of transparent conductive films. As shown in Figure 5e, the theoretical calculated results have a better matching with experimental results at the light transmission of above 80% might attributed to better size accuracy of as-prepared copper grid FCTEs with low copper coverage in our ablation method, which have been reflected clearly in Figure 2 where the copper patterns with bigger line spacings presented more uniform size and smoother copper cutting edge.

For common EMI shielding film, the total EMI SE was usually contributed by the reflection (SE_R), absorption (SE_A), and multiple reflection (SE_M). In our study, the thickness of conductive layer is much less than skin depth, and thus SE_M can be neglected. SE_R and SE_A can be written as follows,

$$SE_R = 10\log\left(\frac{1}{1-R}\right) = 10\log\left(\frac{1}{1-|S_{11}|^2}\right) \quad (10)$$

$$SE_A = 10\log\left(\frac{1-R}{T}\right) = 10\log\left(\frac{1-|S_{11}|^2}{|S_{21}|^2}\right) \quad (11)$$

Figure 5f showed the ratio of the reflected power and absorbed power to the overall incident power. It can be seen the reflection is dominant (>85%) due to high surface conductivity of copper grids. With the sheet resistance decreased, the percentage of the reflected part of electromagnetic wave increased, mainly attributed to increasing mismatched impedance. Further increasing the thickness of copper layer, the EMI SE can be further improved, and the reflectance does not appear to rise obviously may attributed to the increased electromagnetic loss stemmed from residual copper particles (Figure S6e and Figure S6f, Supporting Information). Therefore, such method will become more promising once in combination with other technique, such as chemical etching, for the fabrication of ultrathick copper-based FTCEs. For example, we can first deposit a layer of nanometer-scale thick silver or gold on the surface of copper layer on PET substrate, and then selectively remove the silver or gold layer on copper surface by our laser ablation method to make an etching-resistant noble metal mask, and subsequently we can remove the naked copper by chemical etching, and finally thick copper patterns can be obtained. Large copper layer thickness will further promote EMI SE of flexible transparent conductive films for wider applications.

3. Conclusion

In summary, in this study, we propose a general laser ablation strategy for fabricating robust large-area copper-based flexible electronics. In the whole process, copper patterns with digitally controlled precision and dimension can be produced quickly in one laser scanning pass, without mask and photoresist required. In laser ablation process, the metal layer was removed by heat evaporation, and no obvious damage or structural deformation of polymer substrate was observed due to fast heat dissipation in thin metal layer. Typical copper-based FTCFs and FCBs with different metal layer thicknesses have been manufactured to show the availability of such ablation method in preparing diverse metal-based flexible electronics. The resistance and optical transmittance of as-prepared Cu FTCFs can be readily tuned by controlling the widths, thicknesses, and spacings of copper grids. The optimal optoelectrical performance with light transmission of 90.9% at 550 nm and sheet resistance of 21.6 Ω sq^{-1} was easily achieved, which is comparable to state-of-the-art ITO-based transparent conductors and even better than many other metal nanowires-based FTCFs. The fabricated Cu grid-based FTCEs can be used as the display of an electroluminescent light emitter as well as transparent EMI shielding materials for some special application fields. In addition, UV laser ablation method is also a facile and straightforward approach to produce robust sub-millimeter FCBs, indicating the enormous potential of such method in producing metal-based flexible electronics.

4. Experimental Section

The Preparation of the Copper Clad Polymer Films: In this work, copper-clad polymer films with 100 um thick PET substrate and 200 nm/2 μm thick copper coating layer were principally purchased from commercial company (Teonex Q65FA, Graphene testing and sales platform co. LTD., Taiwan, thickness: 100 μm). Copper layer was coated on a flexible polymer substrate by evaporation or sputtering deposition. The films were used as received without further treatment. Copper adhesion passed ASTM D3359 test.

Laser Ablation: The Copper clad PET films were irradiated with a 3 W diode-pumped Nd: YAG laser with the wavelength of 355 nm which was generated by a second harmonic crystal. The laser spot diameter was ≈8 μm. In a typical laser ablation process for the fabrication of 200 nm thick copper patterns, the laser pulse frequency was set at 30 kHz, the pulse width was set at 30 μs, and the received average laser power on copper surface was measured to be 1.5 W by laser power meter. Furthermore, laser fluence can be controlled by adjusting the half-wave plate in front of the polarized beam splitter, and the other laser parameters were optimized by adjusting the current, frequency, pulse width, etc., for obtaining good laser ablation effect.

Fabrication of the Flexible EL Emitter: The active layer of the EL emitter was composed of electroluminescent (EL) nanoparticles and PDMS elastomer adhesive. ZnS: Cu/Al EL nanoparticles (Shanghai KPT Company) were mixed with the PDMS prepolymer mixture (Sylgard 184 kit, the ratio of PDMS to curing agent is 10:1) with a mass ratio of 2:1. Then, the homogeneous mixture of active EL nanoparticles and PDMS adhesive was spin-coated onto the copper clad PET film at 1000 rpm for 60 s. Subsequently, Cu-based FTCE was pressed on adhesive active EL layer to obtain good contact. The prepared sandwich structure was degassed effectively and cured completely at 80 °C for 12 h in vacuum oven. Thereafter, the device was picked out after cooling to room temperature, and the two-side electrodes were led out separately using conductive copper tapes to connect with an external AC voltage supply (DG2-3-T, Shanghai KPT Company) for the test of EL emission performance.

Characterization: The optical transmittance and sheet resistance of the Cu metallic grid transparent electrodes were measured by a UV–vis spectrophotometer (UV-2600, SHIMADZU) with the setup of an integrating sphere and a four-point probe (SB120, Yangzhou subo electric co. LTD, China). The sheet resistance of the samples was the

average value of 10 measurements. The metallic grid structure of the Cu FTCEs and the thickness of Cu film was characterized using a field-emission scanning electron microscope (FE-SEM; ZEISS SUPRA55, Germany). The optical microscope images of the Cu metallic grid electrodes were obtained using transparent reflectance polarizing microscope (59XC-PC, Shanghai optical instrument factory, Shanghai, China). XRD data of Cu FTCEs was recorded using X-ray diffractometer (D8 ADVANCE, Brooker, Germany). EMI SE of copper grid FTCEs was measured by vector network analyzer (ZVB 40, Rohde & Schwarz company, Germany) on a typical waveguide setup.

Supporting Information

Supporting Information is available from the Wiley Online Library or from the author.

Acknowledgements

The work was supported by the National Key R&D Program of China (Grant No. 2016YFE0204200), the National Natural Science Foundation of China (NSFC, Grant No. 51702009 and 21771017) and Fundamental Research Funds for the Central Universities.

Conflict of Interest

The authors declare no conflict of interest.

Keywords

EMI shielding, flexible circuit boards, flexible transparent electrodes, laser ablation, wearable electronics

Received: April 10, 2019
Revised: July 13, 2019
Published online: August 6, 2019

[1] J. L. Wang, M. Hassan, J. W. Liu, S. H. Yu, *Adv. Mater.* **2018**, *30*, 1803430.
[2] J. Luo, Y. Yao, X. Duan, T. Liu, *J. Mater. Chem. C* **2018**, *6*, 4727.
[3] N. T. Garland, E. S. McLamore, N. D. Cavallaro, D. Mendivelso-Perez, E. A. Smith, D. Jing, J. C. Claussen, *ACS Appl. Mater. Interfaces* **2018**, *10*, 39124.
[4] A. F. Carvalho, A. J. S. Fernandes, C. Leitão, J. Deuermeier, A. C. Marques, R. Martins, E. Fortunato, F. M. Costa, *Adv. Funct. Mater.* **2018**, 1805271.
[5] G. Schwartz, B. C.-K. Tee, J. Mei, A. L. Appleton, D. H. Kim, H. Wang, Z. Bao, *Nat. Commun.* **2013**, *4*, 1859.
[6] W. Song, J. Zhu, B. Gan, S. Zhao, H. Wang, C. Li, J. Wang, *Small* **2018**, *14*, 1702249.
[7] J. Ye, H. Tan, S. Wu, K. Ni, F. Pan, J. Liu, Z. Tao, Y. Qu, H. Ji, P. Simon, Y. Zhu, *Adv. Mater.* **2018**, *30*, 1801384.
[8] Y. Dong, S. S. K. Mallineni, K. Maleski, H. Behlow, V. N. Mochalin, A. M. Rao, Y. Gogotsi, R. Podila, *Nano Energy* **2018**, *44*, 103.
[9] S. Han, S. Hong, J. Ham, J. Yeo, J. Lee, B. Kang, P. Lee, J. Kwon, S. S. Lee, M. Y. Yang, S. H. Ko, *Adv. Mater.* **2014**, *26*, 5808.
[10] H. Seo, H. Kim, J. Lee, M. Park, S. Jeong, Y. Kim, S. Kwon, T. Han, S. Yoo, T. Lee, *Adv. Mater.* **2017**, *29*, 1605587.
[11] S. Mitra, A. Aravindh, G. Das, Y. Pak, I. Ajia, K. Loganathan, E. Di Fabrizio, I. S. Roqan, *Nano Energy* **2018**, *48*, 551.
[12] Y. Li, L. Meng, Y. Yang, G. Xu, Z. Hong, Q. Chen, J. You, G. Li, Y. Yang, Y. Li, *Nat. Commun.* **2016**, *7*, 10214.
[13] S. Ye, A. R. Rathmell, Z. Chen, I. E. Stewart, B. J. Wiley, *Adv. Mater.* **2014**, *26*, 6670.
[14] S. Han, Y. Chae, J. Y. Kim, Y. Jo, S. S. Lee, S. H. Kim, K. Woo, S. Jeong, Y. Choi, S. Y. Lee, *J. Mater. Chem. C* **2018**, *6*, 4389.
[15] S. An, H. S. Jo, D. Kim, H. J. Lee, B. Ju, S. S. Al-deyab, J. Ahn, Y. Qin, M. T. Swihart, A. L. Yarin, S. S. Yoon, *Adv. Mater.* **2016**, *28*, 7149.
[16] P. Hsu, D. Kong, S. Wang, H. Wang, A. J. Welch, H. Wu, *J. Am. Chem. Soc.* **2014**, *136*, 10593.
[17] H. Wu, L. Hu, M. W. Rowell, D. Kong, J. J. Cha, J. R. Mcdonough, J. Zhu, Y. Yang, M. D. Mcgehee, Y. Cui, *Nano Lett.* **2010**, *10*, 4242.
[18] J. H. Park, G. Hwang, S. Kim, J. Seo, H. Park, K. Yu, T. Kim, K. J. Lee, *Adv. Mater.* **2017**, *29*, 1603473.
[19] M. Hu, J. Gao, Y. Dong, K. Li, G. Shan, S. Yang, R. K. Li, *Langmuir* **2012**, *28*, 7101.
[20] D. Lee, D. Paeng, H. K. Park, C. P. Grigoropoulos, *ACS Nano* **2014**, *8*, 9807.
[21] S. Hong, J. Yeo, G. Kim, D. Kim, H. Lee, J. Kwon, H. Lee, P. Lee, S. H. Ko, *ACS Nano* **2013**, *7*, 5024.
[22] W. Shou, B. K. Mahajan, B. Ludwig, X. Yu, J. Staggs, *Adv. Mater.* **2017**, *29*, 1700172.
[23] W. Zhao, T. Rovere, D. Weerawarne, G. Osterhoudt, N. Kang, P. Joseph, J. Luo, B. Shim, M. Poliks, C. Zhong, *ACS Nano* **2015**, *9*, 6168.
[24] J. Cai, C. Zhang, A. Khan, L. Wang, W. Li, *ACS Appl. Mater. Interfaces* **2018**, *10*, 28754.
[25] L. Chang, X. Zhang, Y. Ding, H. Liu, M. Liu, L. Jiang, *ACS Appl. Mater. Interfaces* **2018**, *10*, 29010.
[26] T. Gao, B. Wang, B. Ding, J. Lee, P. W. Leu, *Nano Lett.* **2014**, *14*, 2105.
[27] Y. Han, H. Zhong, N. Liu, Y. Liu, J. Lin, P. Jin, *Adv. Electron. Mater.* **2018**, *4*, 1800156.
[28] C. Zhang, A. Khan, J. Cai, C. Liang, Y. Liu, J. Deng, S. Huang, G. Li, W. Li, *ACS Appl. Mater. Interfaces* **2018**, *10*, 21009.
[29] L. J. Li, B. Zhang, B. Zou, R. Xie, T. Zhang, S. Li, B. Zheng, J. Wu, J. Weng, W. Zhang, W. Huang, F. Huo, *ACS Appl. Mater. Interfaces* **2017**, *9*, 39110.
[30] J. H. M. Maurer, L. González-García, B. Reiser, I. Kanelidis, T. Kraus, *Nano Lett.* **2016**, *16*, 2921.
[31] Y-K. Liu, M-T. Lee, *ACS Appl. Mater. Interfaces* **2014**, *6*, 14576.
[32] H. Kim, M. Song, J. Jeong, C. Su, S. Surabhi, J. Jeong, D. Kim, D. Choi, *J. Power Sources* **2016**, *331*, 22.
[33] O. Thomas, A. K. Schuppert, M. Hummelga, J. Backstrom, H-E. Nilsson, H. Olin, *ACS Appl. Mater. Interfaces* **2015**, *7*, 18273.
[34] Y. Lee, W. Jin, K. Y. Cho, J. Kang, J. Kim, *J. Mater. Chem. C* **2016**, *4*, 7577.
[35] R. Gupta, S. Walia, M. Hosel, J. Jensen, G. Angmo, F. C. Krebs, G. U. Kulkarni. *J. Mater. Chem. A* **2014**, *2*, 10930.
[36] J. H. Park, D. Y. Lee, Y. Kim, J. K. Kim, J. H. Lee, J. H. Park, T. Lee, J. H. Cho, *ACS Appl. Mater. Interfaces* **2014**, *6*, 12380.
[37] W. Zhou, J. Chen, Y. Li, D. Wang, J. Chen, X. Feng, Z. Huang, R. Liu, X. Lin, H. Zhang, B. Mi, Y. Ma, *ACS Appl. Mater. Interfaces* **2016**, *8*, 11122.
[38] D. Paeng, J. Yoo, J. Yeo, D. Lee, E. Kim, S. H. Ko, C. P. Grigoropoulos, *Adv. Mater.* **2015**, *27*, 2762.
[39] J. F. Ready, *Industrial Applications of Lasers*Academic Press, San Diego, CA **1997**.
[40] T. H. Duong, N. H. Tran, H. C. Kim, *Thin Solid Films* **2017**, *622*, 17.
[41] Z. Yin, S. K. Song, S. Cho, D. J. You, J. Yoo, S. T. Chang, Y. S. Kim, *Nano Res.* **2017**, *10*, 3077.
[42] H. Guo, N. Lin, Y. Chen, Z. Wang, Q. Xie, T. Zheng, N. Gao, S. Li, J. Kang, D. Cai, D. L. Peng, *Sci. Rep.* **2013**, *3*, 2323.
[43] S. R. Ye, A. R. Rathmell, I. E. Stewart, Y. C. Ha, A. R. Wilson, Z. F. Chen, B. J. Wiley, *Chem. Commun.* **2014**, *50*, 2562.

[44] H. G. Im, S. H. Jung, J. Jin, D. Lee, J. Lee, D. Lee, J. Y. Lee, I. D. Kim, B. S. Bae, *ACS Nano* **2014**, *8*, 10973.
[45] Y. Zhou, L. Hu, G. Grüner, *Appl. Phys. Lett.* **2006**, *88*, 123109.
[46] S. De, T. M. Higgins, P. E. Lyons, E. M. Doherty, P. N. Nirmalraj, W. J. Blau, J. J. Boland, J. N. Coleman, *ACS Nano* **2009**, *3*, 1767.
[47] J. Y. Lee, S. T. Connor, Y. Cui, P. Peumans, *Nano Lett.* **2008**, *8*, 689.
[48] S. Bae, H. Kim, Y. Lee, X. Xu, J. Park, Y. Zheng, J. Balakrishnan, T. Lei, H. R. Kim, Y. Il Song, Y. Kim, K. S. Kim, *Nature Nanotechnol.* **2010**, *5*, 574.
[49] J. Li, L. Hu, L. Wang, Y. Zhou, G. Grüner, T. J. Marks, *Nano Lett.* **2006**, *6*, 2472.
[50] Z. Yu, Q. Zhang, L. Li, Q. Chen, X. Niu, J. Liu, Q. Pei, *Adv. Mater.* **2011**, *23*, 664.
[51] J. H. Park, D. Y. Lee, Y. H. Kim, J. K. Kim, J. H. Lee, J. H. Park, T. W. Lee, J. H. Cho, *ACS Appl. Mater. Interfaces* **2014**, *6*, 12380.
[52] T. Qiu, B. Luo, M. Liang, J. Ning, B. Wang, X. Li, L. Zhi, *Carbon* **2015**, *81*, 232.
[53] M.-S. Cao, X.-X. Wang, M. Zhang, J.-C. Shu, W.-Q. Cao, H.-J. Yang, X.-Y. Fang, J. Yuan, *Adv. Funct. Mater.* **2019**, *29*, 1807398.
[54] M. Hu, N. Zhang, G. Shan, J. Gao, J. Liu, K. Y. Li Robert, *Front. Phys.* **2018**, *13*, 138113.
[55] J. Jung, H. Lee, I. Ha, H. Cho, K. K. Kim, J. Kwon, P. Won, S. Hong, S. H. Ko, *ACS Appl. Mater. Interfaces* **2017**, *9*, 44609.
[56] M.-S. Cao, W.-L. Song, Z.-L. Hou, B. Wen, J. Yuan, *Carbon* **2010**, *48*, 788.
[57] N. F. Colaneri, L. W. Shacklette, *IEEE Trans. Instrum. Meas.* **1992**, *41*, 291.
[58] L. Jia, D. Yan, X. Liu, R. Ma, H. Wu, Z. Li, *ACS Appl. Mater. Interfaces* **2018**, *10*, 11941.

